GYROKINETIC THEORY OF DRIFT WAVES IN NEGATIVE SHEAR TOKAMAKS

Y. IDOMURA 1), S. TOKUDA 1), Y. KISHIMOTO 1), and M. WAKATANI 2)
1) Naka Fusion Research Establishment,
Japan Atomic Energy Research Institute, Naka, Ibaraki, 311-0193, Japan
2) Graduate School of Energy Science, Kyoto University, Uji, Kyoto, 611-0011, Japan

e-mail contact of main author: idomuray@fusion.naka.jaeri.go.jp

Abstract. Linear and nonlinear properties of slab drift waves in the negative sheared slab configuration modeling the $q_{\min}$-surface region of negative shear tokamaks are studied, where $q_{\min}$ is the minimum value of a safety factor q. Linear calculations show that both the slab ion temperature gradient driven (ITG) mode and the slab electron temperature gradient driven (ETG) mode become strongly unstable around the $q_{\min}$-surface. Nonlinear simulations are performed for the ETG turbulence which evolves in a much faster time scale than the ITG turbulence. It is found that quasi-steady $E_r \times B$ zonal flows are generated by an inverse wave energy cascade process. Linear stability analyses of the electrostatic Kelvin-Helmholtz (K-H) mode show that the quasi-steady $E_r \times B$ zonal flow profile is closely related to the q-profile or the magnetic shear, which has a stabilizing effect on the K-H mode. It is shown that the microscopic quasi-steady $E_r \times B$ zonal flows arising from the ETG turbulence have a strong stabilizing effect on the slab ITG mode.

1 Introduction

In negative shear tokamaks, the ion thermal diffusivity reduces to the neoclassical level in the internal transport barrier (ITB) region. In this region, the ion temperature gradient driven (ITG) mode and the trapped electron mode are considered to be stabilized by the $E_r \times B$ shear flows. Recently, the electron temperature gradient driven (ETG) mode has been proposed as a candidate for the residual anomalous electron thermal transport in the ITB region [1, 2]. In understanding the transport properties in the ITB, behavior of drift waves in the negative shear configuration must be studied. The negative-sheared slab ITG (NS-ITG) mode [3] and the negative-sheared slab ETG (NS-ETG) mode [4] are analyzed in the $q_{\min}$-surface region using a gyrokinetic integral eigenvalue code [3]. These modes are important even in the toroidal geometry, since a toroidal mode coupling becomes weak around the $q_{\min}$-surface.

Particularly for the NS-ETG mode, which gives a much larger growth rate than the NS-ITG mode, nonlinear behavior is addressed using a gyrokinetic particle-in-cell (PIC) code [5]. As a model for the improved ion confinement, a spontaneous generation of the $E_r \times B$ zonal flow in the ITG turbulence has been reported in a recent work [6]. We have observed a generation of $E_r \times B$ zonal flows also in the ETG turbulence. A stability of the $E_r \times B$ zonal flow is discussed from a point of view of the electrostatic Kelvin-Helmholtz (K-H) instability. Finally, an effect of the ETG driven $E_r \times B$ zonal flows on the ITG turbulence is addressed.

In Sec. 2, linear properties of the NS-ETG and NS-ITG modes are discussed based on the eigenmode structure, the growth rate spectrum, and the transport coefficient obtained from the mixing length estimate. In Sec. 3, a spontaneous generation of $E_r \times B$ zonal flows in a nonlinear simulation of the NS-ETG mode is shown. In Sec. 4, a linear stability of the K-H mode is studied for the $E_r \times B$ zonal flow observed in the simulation. In Sec. 5, a linear stability of the NS-ITG mode under the ETG driven $E_r \times B$ zonal flow is given. In Sec. 6, obtained results are summarized.

2 Linear Stability

In the present study, we consider a sheared slab geometry, where the x-direction corresponds to the radial direction, the z-direction is chosen in the direction of the magnetic field at $x = 0$, and the y-direction is chosen to be normal to both the x and z-direction. For such a slab plasma, we assume the periodic boundary condition in the y and z-direction, and the fixed boundary condition with conducting walls in the x-direction. For the negative shear configuration, we choose the model magnetic configuration as $\mathbf{B}(x) = B_0[\mathbf{z} - (x/L_{ns})^2\mathbf{y}]$, where $L_{ns} = \sqrt{(2q_0^2R)/(q_0''r_0)}$, R is the major radius of a toroidal plasma, r_0 is the minor radius corresponding to the position $x = 0$, and q_0, q_0'' are evaluated at the $q_{\min}$-surface. Parameters used in the present study are chosen based on plasma parameters in Tokamak Fusion Test Reactor (TFTR) [7]: $R = 2.6$m; $r_0 = 0.3$m; the electron and ion density $\bar{n_e} = \bar{n_i} \sim 2 \times 10^{19}\mathrm{m}^{-3}$; the density gradient parameter $L_n = 0.38$m; the electron temperature $\bar{T_e} \sim 3.91$keV; the ion temperature $\bar{T_i} = 12.8$keV; the ion Larmor radius $\bar{\rho}_{ti} = 2.52$mm; the electron Larmor radius $\bar{\rho}_{te} = 0.0325$mm; the electron Debye length $\bar{\lambda}_{De} = 0.104$mm; and the background field $B_0 = 4.6$T, where $\bar{\cdot}$ denotes a quantity averaged over the region of the $q_{\min}$-surface.The model magnetic configuration is given with $L_s = 2.78\mathrm{m}(L_n/L_s = 0.167)$ for the normal shear case, and $L_{ns} = 0.883\mathrm{m}(L_n/L_s = 0.430)$ for the negative shear case.

Figure 1 shows the growth rate spectra and the transport coefficients of the slab ETG and ITG modes obtained from the gyrokinetic integral eigenvalue code. Analytic solutions show that the double mode-rational surface (nonresonant) NS-ITG mode becomes a bounded (oscillatory) solution which is excited in the $q_{\min}$-surface region [4]. Their stabilities are basically determined locally at the $q_{\min}$-surface, because the magnetic shear is weak in the $q_{\min}$-surface region. Since a local stability of the slab mode does not depend on a sign of $k_\parallel$, the double mode-rational surface and nonresonant NS-ITG modes give similar growth rate spectra, provided that $|k_\parallel|$ is the same at the $q_{\min}$-surface, where $k_\parallel = \mathbf{k}\cdot\mathbf{B}/|\mathbf{B}|$. For both the double mode-rational surface and nonresonant NS-ITG modes, unstable k_y regions spread over $k_y\rho_{ti} \sim 10$, because the magnetic shear stabilization does not work around the $q_{\min}$-surface [3]. These modes may explain a short wavelength ion mode observed in the TFTR enhanced reversed shear experiment [8].

The short wavelength ETG mode shows different feature from the ITG mode, because the Debye shielding effect becomes important in typical fusion plasma parameters. In a Weber type differential eigenmode equation which is obtained with retaining the Debye shielding effect, a term which makes an effective potential has the opposite sign compared with that of the ITG mode [4]. Hence, types of solutions are exchanged between the ITG and ETG modes. The double mode-rational surface (nonresonant) NS-ETG mode has an oscillatory (bounded) solution around the $q_{\min}$-surface. As in the case of NS-ITG modes, their stabilities are also determined locally at the $q_{\min}$-surface. However, their unstable k_y regions are characterized by $k_y\lambda_{De} \sim 1$, because of the Debye shielding effect. For parameters used in the present analysis, this unstable k_y region corresponds to $k_y\rho_{te} \sim 0.3$.

The negative sheared slab modes give order of magnitude larger radial correlation lengths and growth rates than the normal-sheared slab modes. The corresponding mixing length estimates give significantly large transport coefficients. In the normal shear case, unstable k_y regions of the ITG mode $k_y\rho_{ti} < 1$ and that of the ETG mode $k_y\lambda_{De} < 1$ are separated. On the other hand, in the negative shear case, their unstable regions overlap each other around $k_y\rho_{ti} \sim 10$ ($k_y\lambda_{De} \sim 0.4$). Since the growth rate of the ETG mode is an order of magnitude larger than that of the ITG mode, effects of the ETG turbulence can not be ignored in considering the ITG turbulence. Especially in the negative shear tokamaks, non-adiabatic electrons are

considered to play a significant role in a formation of a drift-wave turbulence.

3 Nonlinear Simulation of ETG Turbulence

The gyrokinetic PIC simulation is performed for the nonresonant NS-ETG mode, which gives the largest transport coefficient in Fig. 1(b). In the present study, a simulation model with single helicity perturbations and an adiabatic ions is used to reduce a simulation cost.

In Figs. 2(a)-2(d), contour plots of the electrostatic potential are shown for the simulation of the nonresonant NS-ETG mode with $\eta_e = \eta_i = 5$ and $L_{ne}/L_{ns} \sim 0.430$. In the linear phase for $t\Omega_i = 0 \sim 1100$ [see Fig. 2(a)], the radially elongated vortex structure appears. The k_y spectrum in Fig. 3(a) peaks at $k_y\bar{\rho}_{te} = 0.258$ where the maximum linear growth rate is given in Fig. 4(a). The broad radial eigenmode structure is a characteristic feature of the NS-ETG modes which becomes unstable around the $q_{\min}$-surface.

A saturation of the nonresonant NS-ETG mode occurs around $t\Omega_{te} \sim 1100$. In the initial saturation phase [see Fig. 2(b)], the radially elongated vortices are broken into small scale and almost isotropic eddies. A destruction of the radially elongated vortices is caused by $E \times B$ shear flows with $k_y \sim 0$, which is generated by a local charge separation arising from the electron particle transport. This process is recognized as a normal cascade in the k_x space. In Fig. 3(a), we see an inverse cascade process in the k_y space. These properties of the wave energy cascade in a relatively long wavelength regime with $k_\perp \rho_{te} < 1$ are consistent with a picture of a self-organization process in the electrostatic drift-wave turbulence [9]. It is noted that through the whole time evolution, a variation of the electron temperature is estimated as $\delta T_e/T_{0e} \leq 0.005$. A modification of the velocity distribution function due to a particle trapping is weak, because of a small saturation amplitude with $e\phi/T_e \leq 0.003$ in the initial saturation phase. Therefore, an important saturation mechanism is considered to be an inverse (normal) energy cascade process in the k_y (k_x) space which generates $E \times B$ shear flows with $k_y \sim 0$.

After the initial nonlinear saturation of the unstable ETG modes [see Fig. 2(c)], for $t\Omega_i = 1200 \sim 2300$, a low-$k_y$ secondary instability occurs in a linearly stable region in both sides of the nonlinearly saturated region around the $q_{\min}$-surface. The wave number of the secondary instability is estimated as $k_y\bar{\rho}_{te} = 0.0859$ in Fig. 3(b). This unstable k_y region can not be explained by the linear growth rate of the ETG mode which peaks around $k_y\lambda_{De} \sim 1$ ($k_y\bar{\rho}_{te} \sim 0.3$). The k_y spectrum shown in Fig. 3(b) also shows the inverse energy cascade during the evolution of the secondary instability. This inverse energy cascade process leads to a generation of strong $E_r \times B$ zonal flows.

Finally, in the quasi-stationary phase after $t\Omega_i \sim 2400$ [see Fig. 2(d)], the wave energy condenses into the $k_y = 0$ mode, which means a formation of $E_r \times B$ zonal flows. Then, the expansion of the secondary instability region is suppressed. The observed radial profile of the quasi-steady $E_r \times B$ zonal flow is non-uniform and has a fairly large flow velocity ($v_{E_r \times B} \sim 0.015\bar{v}_{ti}$ and $\bar{v}_t$ is the thermal velocity) only in finite magnetic shear regions in both sides of the $q_{\min}$-surface. Although an inverse energy cascade in the k_y space is observed both in the region of the $q_{\min}$-surface [see Fig.3(a)] and in the large $E_r \times B$ zonal flow region [see Fig.3(b)], the wave spectrum condensation into the $k_y = 0$ mode occurs only in the latter region. Since the main difference between these two regions is the magnetic shear, we suppose that the magnetic shear plays a significant role for sustaining the $E_r \times B$ zonal flows. In order to confirm this conjecture, we will discuss about a stability of the $E_r \times B$ zonal flow from a point of view of the K-H instability.

4 Stability of $E \times B$ Zonal Flow

In order to analyze a stability of the $E_r \times B$ zonal flows observed in the simulation, the gyrokinetic integral eigenvalue code is extended to include an equilibrium $E_r \times B$ flow. Since the scale length of flow shear is much larger than the electron Larmor radius, $\bar{\rho}_{te}/L_v \sim O(\varepsilon)$, the gyroaverage for the radial electric field E_r is ignored, and an effect of an equilibrium $E_r \times B$ shear flow is easily incorporated as the Doppler shift for the eigenfrequency.

The stability condition for the K-H mode is estimated analytically by reducing the gyrokinetic integral eigenmode equation into the Rayleigh equation [10] in the limit: $k_\perp \rho_{te} \to 0$, $L_{ne} = L_{ni} \to \infty$, $L_{te} = L_{ti} \to \infty$, $L_{ns} \to \infty$, and $n_{1i} \to 0$, where the ion response n_{1i} is ignored for simplicity [5]. In the Rayleigh equation, a non-dimensional parameter corresponding to the Richardson number in a neutral fluid is given by $J = (k_\parallel L_v/\bar{\lambda}_{De})^2/(k_y v_0/\bar{v}_{te})^2$, where v_0 is a characteristic flow velocity. For the flow profile of $v_{E_r\times B} = v_0 \tanh(x/L_v)$, the marginal stability condition is obtained as $J = k_y^2 L_v^2(1 - k_y^2 L_v^2)$ [11]. From this condition, the K-H mode is completely stabilized for $k_y L_v > 1$ and $k_\parallel L_v > (v_0/\bar{v}_{te})/(2\sqrt{2}L_v/\bar{\lambda}_{De})$.

In the numerical calculation, we have chosen the model $E_r \times B$ flow profile as $v_{E_r\times B}(x) = v_0[x - x_c]/L_v \exp\{-([x-x_c]/L_v)^2/2 + 1/2\}$, where $x = x_c$ is the neutral point of the flow profile. A scale length of flow shear is chosen as $L_v \sim 14.4\bar{\rho}_{te}$ based on the observed $E_r \times B$ zonal flow. Above stability conditions are confirmed also in numerical results. In Fig. 4(a), the growth rate spectrum of the K-H mode for the model $E_r \times B$ flow profile with $v_0 = 0.02\bar{v}_{ti}$ and $x_c = 0$ (x_c is at the $q_{\min}$-surface) is shown. The unstable k_y region of the K-H mode exists in a low k_y side compared with that of the ETG mode, and this region corresponds to the k_y region where the secondary instability occurs.

Since a stabilizing effect on the K-H mode is produced by a variation of $k_\parallel$, it is considered that the $E_r \times B$ zonal flow profile is related to the q-profile. In Figs. 5(a)-5(d), we show time histories of the $E_r \times B$ zonal flow profile in simulations of the nonresonant NS-ETG mode with $\eta_e = \eta_i = 5$ and different q-profiles. In the simulation with $L_{ne}/L_{ns} = 0$ shown in Fig. 5(a), quasi-steady $E_r \times B$ zonal flows are not generated. Also for other three cases, $E_r \times B$ zonal flows are not observed near the $q_{\min}$-surface. In Figs. 5(b)-5(d), a clear correlation between the $E_r \times B$ zonal flow profile and the q-profile is observed. The linear stability of the K-H mode is analyzed for the configurations used for Figs. 5(b)-5(d). In Fig. 4(b), a critical $E_r \times B$ flow velocity v_{0c} to stabilize the K-H mode is plotted for the model $E_r \times B$ flow profiles with various neutral points x_c. This result explain the feature of the $E_r \times B$ zonal flow profile observed in the simulation qualitatively. It is noted that a flow damping effect due to a dissipation such as a Coulomb collision is not involved in the present simulation, because the growth time of the ETG mode is shorter than that of the ITG mode. Therefore, $E_r \times B$ flows which are stable for the K-H mode are sustained for a long time. The observed quasi-steady state with $E_r \times B$ zonal flows is considered as a stable equilibrium solution of the gyrokinetic Vlasov-Maxwell system.

From obtained results, properties of the secondary instability are summarized as follows: (a) the instability occurs in the neighborhood of the $E \times B$ shear flow or $E_r \times B$ zonal flow region, (b) the most unstable k_y region, $k_y\bar{\rho}_{te} \sim 0.1$, is much lower than that of the ETG mode, $k_y\bar{\rho}_{te} \sim 0.3$, (c) after the saturation of the instability, the $E_r \times B$ zonal flow is generated, provided that $k_\parallel$ is sufficiently large, and (d) the instability propagates only in the weak magnetic shear region with $k_\parallel\bar{\rho}_{te} < 10^{-5}$. From these properties, it is considered that the secondary instability is the K-H mode, which becomes unstable in a front of the $E \times B$ shear flow or $E_r \times B$ zonal flow region. The propagation of the secondary instability may correspond to an avalanche process produced by a chain of the K-H instability and an associated generation of the $E_r \times B$ zonal flow.

5 Linear Stability of ITG Mode in ETG Turbulence

The last problem addressed in this work is a stability of the ITG mode in the presence of the ETG turbulence. As is seen in Fig. 1, the linear growth rate of the ETG mode is an order of magnitude larger than that of the ITG mode. In studying the ITG turbulence, it is necessary to consider effects of the ETG turbulence even for the linear stability. In this paper, we study an effect of the $E_r \times B$ zonal flow, which is generated from the ETG turbulence, on the ITG turbulence. In this section, we consider the gyrokinetic ions under microscopic equilibrium $E_r \times B$ zonal flows as a model configuration. It is noted that although simulations shown in Sec. 3 assume an adiabatic ion response, we have observed a generation of $E_r \times B$ zonal flows also in a simulation with the gyrokinetic ions.

For the gyrokinetic ions, the scale length ordering is estimated as $\rho_{ti}/L_v \sim O(1)$, and the FLR effect becomes important also for the equilibrium $E_r \times B$ shear flow. This treatment in the gyrokinetic integral eigenvalue code becomes very complicated because a velocity integral of the plasma dispersion function requires an integration also about the magnetic moment. Thus, we have developed a new initial value code based on the gyrokinetic particle simulation technique. In order to treat the full FLR effect in the gyrokinetic particle simulation, we assign a particle density and impose the consistency condition in the Fourier space where the FLR effect is expressed analytically with the zeroth order Bessel function. As in the gyrokinetic integral eigenvalue code, the gyrokinetic Poisson equation, which is formulated as an integral equation, is solved in the Fourier space with retaining the full FLR effect.

The calculation is performed for the $l = 0$ branch of the double mode-rational surface NS-ITG mode with the same parameters as in Fig. 1. In the linear calculation of the ITG mode, electron modes are ignored by assuming the adiabatic electron response. A model $E_r \times B$ zonal flow profile is chosen as the sinusoidal function, $v_{E_r\times B}(x) = v_0 \sin([\pi/2L_v]x)$, where the flow shear parameter is $L_v \sim 16.7\bar{\rho}_{te}$ ($\bar{\rho}_{ti}/L_v \sim 4.59$). Figures 6 shows the v_0-dependence of the eigenfrequency. While the real frequency is insensitive to a change in v_0, the microscopic $E_r \times B$ zonal flow is remarkably effective for stabilizing the NS-ITG mode. The marginally stable condition is given in a very small $E_r \times B$ flow velocity with $v_0/\bar{v}_{ti} \sim 0.005$. In order to understand the stabilizing mechanism, the resonance condition, $|k_\parallel|v_{ti}/|\mathrm{Re}(\omega) - k_y\langle v_{E_r\times B}\rangle_{\bar{\theta}}|$, is plotted for the cases with and without the $E_r \times B$ zonal flow in Fig. 7, where the gyro-average is evaluated for thermal ions, $\langle v_{E_r\times B}\rangle_{\bar{\theta}} = v_0 \sin([\pi/2L_v]x)J_0([\pi/2L_v]\rho_{ti})$. Since the real frequency is almost constant, the resonance condition is not changed on average. However, in a wide range of the unstable region around the $q_{\min}$-surface, the local resonance condition is shifted from the most unstable condition due to the Doppler shift with the microscopic $E_r \times B$ zonal flow. This property that the resonance condition is shifted without changing the real frequency is a unique stabilizing mechanism of the microscopic $E_r \times B$ zonal flow. It is noted that such a strong stabilizing effect can not be expected for the global $E_r \times B$ shear flow, because the real frequency is also shifted to sustain the instability.

6 Discussion

In this work, we have analyzed linear and nonlinear properties of micro-instabilities particularly for the negative shear configuration, based on the gyrokinetic theory. Linear calculations show that in a weak magnetic shear region around the $q_{\min}$-surface, the NS-ETG and NS-ITG modes become strongly unstable, and their transport coefficients based on the mixing length theory are an order of magnitude larger than those obtained in the normal shear configuration. This result suggests a possibility of a large electron anomalous transport in the ITB region based

on the ETG mode.

In nonlinear simulations of the ETG turbulence, a formation of $E_r \times B$ zonal flows due to an avalanche process of the K-H like secondary instability and an inverse wave energy cascade is observed. From stability analyses of the observed $E_r \times B$ zonal flow, it is found that a final state of the $E_r \times B$ zonal flow profile is determined by a stability of the K-H mode. Linear calculation of the ITG mode under a model $E_r \times B$ flow show that, if the ETG driven microscopic $E_r \times B$ zonal flows are sustained for a long time, the ITG turbulence is easily suppressed. Therefore, it is considered that the ETG turbulence play a significant role in determining a transport property in the ITB region of negative shear tokamaks.

Acknowledgments

The numerical computations in this work were performed on COMplex PArallel Computer System (COMPACS) of the Center for Promotion of Computational Science and Engineering, JAERI, VPP500 system of Tokai Research Establishment, JAERI, and Paragon XP/S-75MP834 system of Kansai Research Establishment, JAERI.

References

[1] STEABLER, G. M., *et al.*, in *Plasma Physics and Controlled Nuclear Fusion Research 1998*, 17th IAEA Fusion Energy Conference, Yokohama, Japan, 1998 (International Atomic Energy Agency, Vienna, 1998), p. F1-CN-69/THP2/13.

[2] STALLARD, B. W., *et al.*, Phys. Plasmas **6**, 1978 (1999).

[3] IDOMURA, Y., TOKUDA, S., and WAKATANI, M., Phys. Plasmas **6**, 4658 (1999).

[4] IDOMURA, Y., TOKUDA, S., and WAKATANI, M., Phys. Plasmas **7**, 2456 (2000).

[5] IDOMURA, Y., TOKUDA, S., and WAKATANI, M., Phys. Plasmas **7**, 3551 (2000).

[6] LIN, Z., *et al.*, Science, **281**, 1835 (1998).

[7] HAWRYLUK, R. J., *et al.*, Phys. Plasmas **5**, 1577 (1998).

[8] WONG, K. L., *et al.*, Phys. Lett. A **236**, 339 (1997).

[9] HASEGAWA, A., Adv. Phys. **34**, 1 (1985).

[10] CHANDRASEKHAR, S., *Hydrodynamic and Hydromagnetic Stability*, (Clarendon, Oxford, 1961).

[11] DRAZIN, P. G., J. Fluid Mech. **4**, 214 (1958).

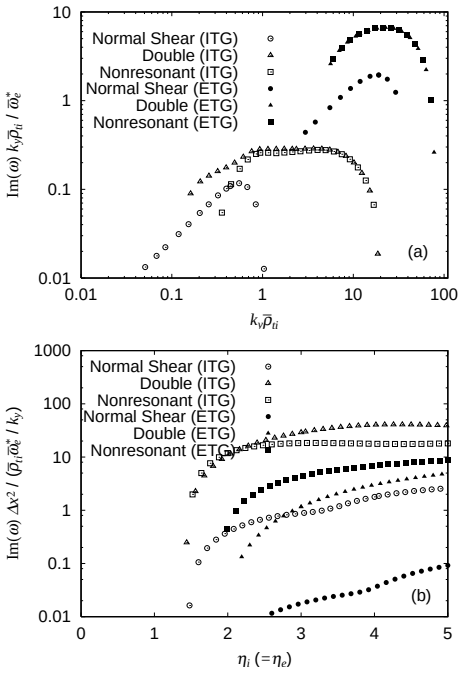

FIG 1: (a) The growth rate spectra of the slab ETG and ITG modes with $\eta_e = \eta_i = 5$. (b) The corresponding transport coefficients estimated from the mixing length theory. Wavenumbers are chosen so that the critical η_i $(= \eta_e)$ becomes an minimum value.

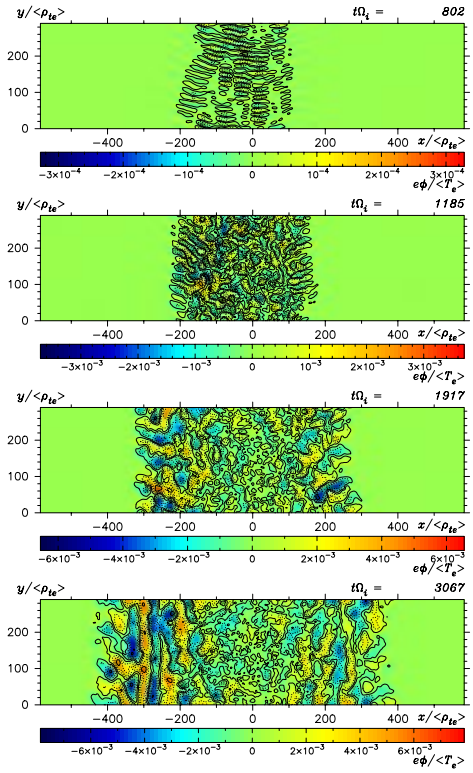

FIG 2: Contour plots of ϕ are shown for the simulation of the nonresonant NS-ETG mode with $\eta_e = \eta_i = 5$ and $L_{ne}/L_{ns} \sim 0.430$. The $q_{\min}$-surface is $x/\bar{\rho}_{te} = 0$.

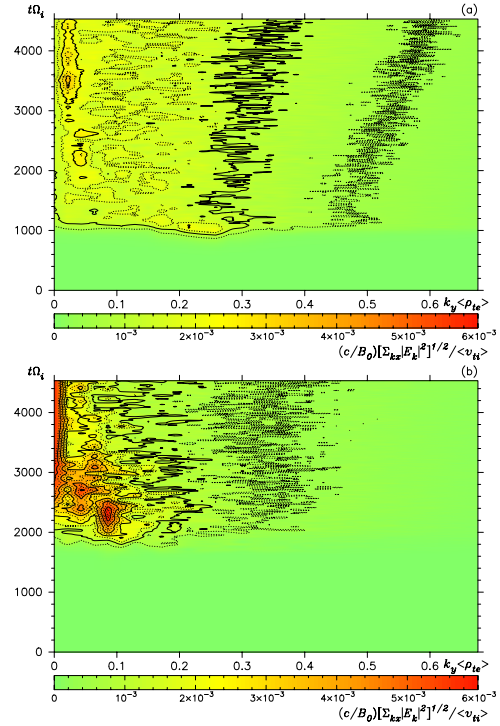

FIG 3: Time histories of k_y wave energy spectrum observed in the simulation shown in Fig. 2. The observation regions are set for (a) $x/\bar{\rho}_{te} = -146.2 \sim 146.2$ and (b) $x/\bar{\rho}_{te} = -361.1 \sim -287.9$.

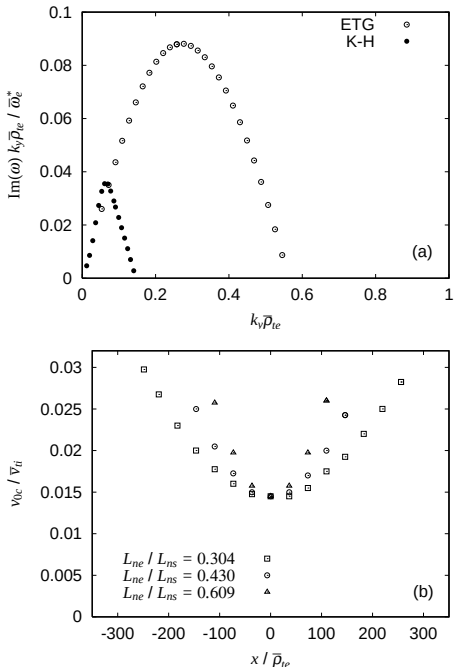

FIG 4: (a) The growth rate spectra of the K-H and ETG mode in the single-helicity configuration with $L_{ne}/L_{ns} = 0.430$. (b) The critical $E_r \times B$ flow velocity v_{0c} of the K-H mode for the negative shear configuration in Figs. 5(b)-5(d).

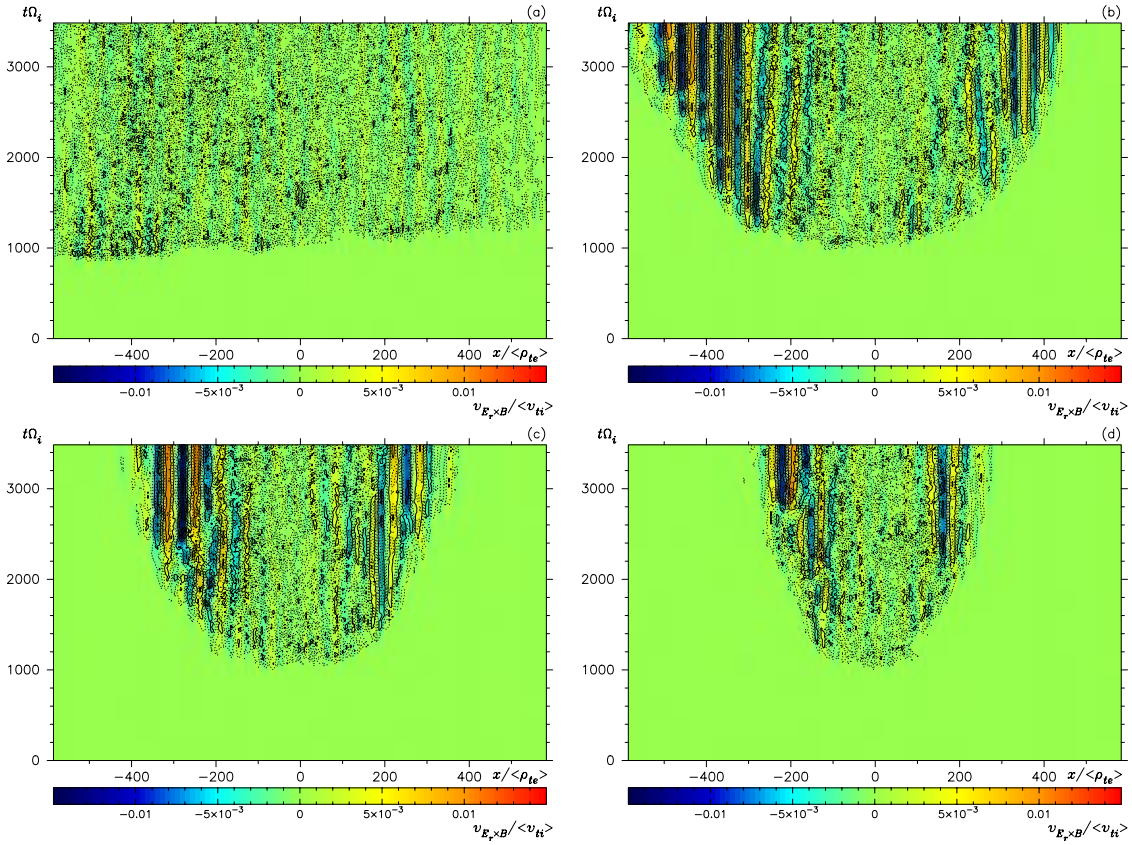

FIG 5: Time histories of the radial distribution of $v_{E_r\times B}$ observed in the simulation of the nonresonant NS-ETG mode with (a) $L_{ne}/L_{ns}=0$, (b) $L_{ne}/L_{ns}=0.304$, (c)$L_{ne}/L_{ns}=0.430$, and (d) $L_{ne}/L_{ns}=0.609$.

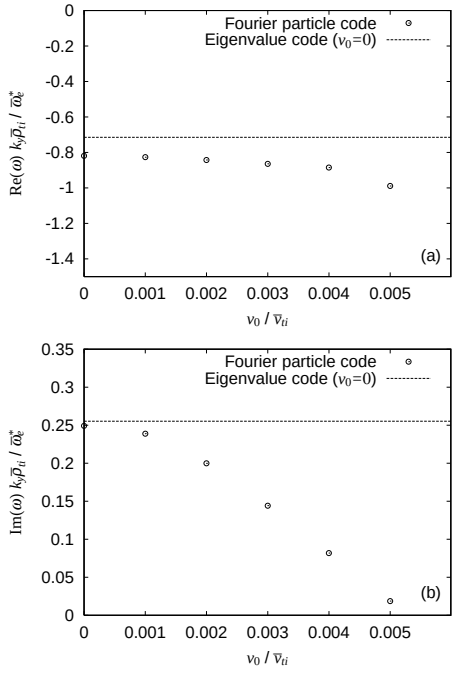

FIG 6: (a) Real frequency and (b) growth rate of the $l=0$ branch of the double mode-rational surface NS-ITG mode are plotted against $v_0/\bar{v}_{ti}$.

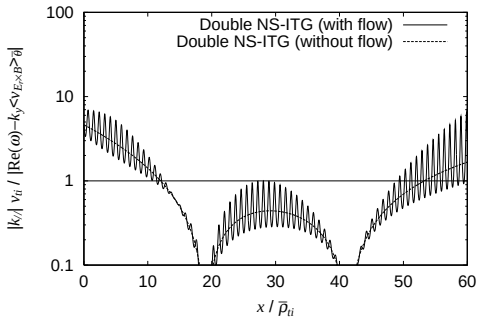

FIG 7: Resonance conditions with $(v_0/\bar{v}_{ti}=0.004)$ and without $(v_0=0)$ the $E_r\times B$ zonal flow are compared. In the case with the $E_r\times B$ zonal flow, the gyro-average is evaluated for thermal ions with $\rho_i=\rho_{ti}$.